Chapter 6

Competing Orders, Quantum Phase Fluctuations, and Quasiparticle Tunneling Spectra

6.1 Introduction

In the previous two chapters, we have presented the scanning tunneling spectroscopic studies of hole-doped YBCO [§4] and electron-doped SLCO [§5] that reveal several contrasting spectroscopic features. Specifically, the quasiparticle tunneling spectra of YBCO exhibit spectral characteristics well captured by the mean-field d-wave [or $(d+s)$-wave] generalized BTK formalism. In SLCO, the quasiparticle tunneling spectra are consistent with isotropic s-wave pairing symmetry while excess low-energy spectral weight that deviates significantly from the mean-field BCS theory is present. In accordance with the low-energy spectral anomaly, high-field low-temperature vortex dynamics measurements on SLCO reveal sizable reduction of H_{irr}^{ab} with respect to H_{c2}^{ab} at $T \rightarrow 0$, implying strong field-induced quantum phase fluctuations. In comparison, relatively weaker quantum phase fluctuations associated with YBCO is consistent with the applicability of mean-field theory to its low-energy spectral characteristics. The satellite features and the "pseudogap"-like spectral dip around the Fermi level manifested in the tunneling spectra of p-type cuprates are suggestive of the presence of a pinned competing order with an energy scale comparable to or larger than that of superconductivity. On the other hand, the complete absence of the satellite features and zero-field pseudogap, and the appearance of current- or field-induced "pseudogap" in n-type SLCO and other

one-layer compounds signify a small coexisting competing order revealed only upon the suppression of superconductivity. Based on these findings and the notion that the varying degrees of quantum phase fluctuations are indicative of the varying degrees of proximity to quantum criticality, we conjecture that the non-universal spectral features among n- and p-type cuprates can be accounted for by tuning the relative energy scales of competing orders to superconductivity.

In this chapter, the aforementioned conjecture is put to test by means of a calculation of the low-energy single-particle spectra that incorporates quantum phase fluctuations into superconductivity with coexisting density waves as the competing order. To date, most theoretical investigations on the tunneling spectra of cuprate superconductors generally address competing orders and superconducting phase fluctuations separately. One approach takes the BCS-like Hamiltonian as the unperturbed mean-field state and treats the disorder-pinned competing order as the weak perturbative scattering potential for the Bogoliubov quasiparticles [249, 255, 256, 257, 258, 259, 260, 101, 261] [§6.3]. Another approach begins with the BCS-like Hamiltonian and includes superconducting phase fluctuations in the proper self-energy correction without any consideration of competing orders [262, 263, 264]. By allowing both the competing orders and the superconducting phase fluctuations in the superconducting state [§6.2], we find that the low-energy excitations thus derived differ from conventional Bogoliubov quasiparticles, and various seemingly puzzling and non-universal phenomena in the hole- and electron-type cuprates, such as the excess subgap low-energy excitations [§5.3.1] below T_c and pseudogap phenomena [§5.4.3], can be coherently explained. We further consider the low-energy limit in d-wave superconductors where the Bogoliubov quasiparticles are the dominating low-energy excitations and disorder-pinned competing orders maybe treated perturbatively, and find that calculated quasiparticle interference spectra reveal modulated density of states due to the presence of competing order, consistent with experimental observations. Therefore, we conclude that the presence of competing orders is indisputable at least in the quasi-2D Bi-2212.

6.2 Competing orders and quantum phase fluctuations on low-energy excitations

We first consider a simple case of coexisting s-wave superconductivity (SC) and charge density waves (CDW) with finite quantum phase fluctuations at $T = 0$. That charge density wave is the relevant competing order to s-wave superconductivity is because the symmetry of s-wave superconducivity is compatible with that of CDW. Under certain conditions, such as in the half-filled Hubbard model with negative U, the two orders can further rotate into each other without modifying the low-energy spectrum and hence be unified under a higher SO(4) symmetry [265]. Empirically, the coexistence has been known in $NbSe_2$ [266, 267], although the energy scale of CDW in $NbSe_2$ is much larger than that of superconductivity and therefore does not directly affect the low-energy excitations of the superconducting order. The simple case of s-wave superconductivity coexisting with CDW can be extended straightforwardly to $d_{x^2-y^2}$-wave superconductivity with a competing order being either CDW [252, 73], spin-density waves (SDW) [268, 249], or d-density waves (DDW) [75]. Nevertheless, compatibility in the symmetry of the superconductivity order parameter with that of the relevant competing order is important for determining which competing states is pertinent under a given superconducting pairing symmetry.

In subsequent discussions we shall associate realistic band structures of n-type cuprate superconductors with the scenario of coexisting s-wave SC and CDW, and those of p-type cuprates with the scenario of coexisting $d_{x^2-y^2}$-wave SC with disorder-pinned SDW. We further assume that the exact degree of quantum phase fluctuations depends on microscopic coupling mechanism between superconductivity and competing orders, which is not fully understood and is therefore left as a variable to be determined empirically.

6.2.1 Formalism

In the case of coexisting s-wave SC and CDW, the mean-field Hamiltonian is given by:

$$\begin{aligned}
\mathcal{H}_{MF} &= \mathcal{H}_{SC} + \mathcal{H}_{CDW} \\
&= \textstyle\sum_{\mathbf{k},\sigma}\ \xi_{\mathbf{k}}\ c^{\dagger}_{\mathbf{k},\sigma} c_{\mathbf{k},\sigma} - \ \sum_{\mathbf{k}}\ \Delta\ \left(c^{\dagger}_{\mathbf{k},\uparrow} c^{\dagger}_{-\mathbf{k},\downarrow} + \ c_{-\mathbf{k},\downarrow} c_{\mathbf{k},\uparrow} \right) \\
&\quad + \textstyle\sum_{\mathbf{k},\sigma}\ V\ \left(c^{\dagger}_{\mathbf{k},\sigma} c_{\mathbf{k}+\mathbf{Q},\sigma} + \ c^{\dagger}_{\mathbf{k}+\mathbf{Q},\sigma} c_{\mathbf{k},\sigma} \right) \\
&= \textstyle\sum_{\mathbf{k}} \left(c^{\dagger}_{\mathbf{k},\uparrow}\ c_{-\mathbf{k},\downarrow}\ c^{\dagger}_{\mathbf{k}+\mathbf{Q},\uparrow}\ c_{-(\mathbf{k}+\mathbf{Q}),\downarrow} \right)
\begin{pmatrix}
\xi_{\mathbf{k}} & -\Delta & -V & 0 \\
-\Delta & -\xi_{\mathbf{k}} & 0 & V \\
-V & 0 & \xi_{\mathbf{k}+\mathbf{Q}} & -\Delta \\
0 & V & -\Delta & -\xi_{\mathbf{k}+\mathbf{Q}}
\end{pmatrix}
\begin{pmatrix}
c_{\mathbf{k},\uparrow} \\
c^{\dagger}_{-\mathbf{k},\downarrow} \\
c_{\mathbf{k}+\mathbf{Q},\uparrow} \\
c^{\dagger}_{-(\mathbf{k}+\mathbf{Q}),\downarrow}
\end{pmatrix} \\
&\equiv \textstyle\sum_{\mathbf{k}}\ \Psi^{\dagger}_{\mathbf{k},\mathbf{Q}}\ H_0\ \Psi_{\mathbf{k},\mathbf{Q}},
\end{aligned}$$

where $\xi_{\mathbf{k}}$ is the normal-state energy of particles of momentum $\mathbf{k}$ relative to the Fermi energy, σ is the spin index, $c^{\dagger}$ and c are the fermion creation and annihilation operators, $\mathbf{Q}$ is the wave vector of the CDW, and Δ and V denote the SC energy gap and CDW energy scale, respectively. H_0 is the (4×4) matrix, and the adjoint of Ψ represents a (1×4) matrix $\Psi^{\dagger}_{\mathbf{k},\mathbf{Q}} \equiv \left(c^{\dagger}_{\mathbf{k},\uparrow}\ c_{-\mathbf{k},\downarrow}\ c^{\dagger}_{\mathbf{k}+\mathbf{Q},\uparrow}\ c_{-(\mathbf{k}+\mathbf{Q}),\downarrow} \right)$. We have further imposed the condition $\xi_{\mathbf{k}}\xi_{-(\mathbf{k}+\mathbf{Q})} < 0$ to ensure that CDW excitations only involve particle-hole sectors. The mean-field Hamiltonian in Eq. (6.1) can be exactly diagonalized so that the bare Green's function $G_0(\mathbf{k},\omega)$ is given by

$$G_0^{-1} = \omega I - H_0 = \begin{pmatrix}
\omega - \xi_{\mathbf{k}} & \Delta & V & 0 \\
\Delta & \omega + \xi_{\mathbf{k}} & 0 & -V \\
V & 0 & \omega - \xi_{\mathbf{k}+\mathbf{Q}} & \Delta \\
0 & -V & \Delta & \omega + \xi_{\mathbf{k}+\mathbf{Q}}
\end{pmatrix}, \tag{6.1}$$

where I denotes the (4×4) unit matrix.

Next, we introduce phase fluctuations to the superconducting order parameter $\Delta(\mathbf{r}) = |\Delta(\mathbf{r})|\, e^{i\theta(\mathbf{r})}$. In order to couple quasiparticles explicitly to the phase field $\theta(\mathbf{r})$, we follow Ref. [262] and perform

a gauge transformation to the fermion operators: $c_\sigma(\mathbf{r}) \to c_\sigma(\mathbf{r})e^{i\theta(\mathbf{r})/2}$. After integrating out the fast momentum degrees of freedom with variations larger than $1/\xi_0$ (ξ_0: superconducting coherence length) [269], the resulting low-energy effective theory contains the mean-field theory of coexisting SC and CO, the Gaussian theory of the phase fluctuations, and the coupling term between the two [262]:

$$\begin{aligned} \mathcal{H}_{eff} &= \mathcal{H}_0 + \mathcal{H}_I, \\ \mathcal{H}_0 &= \mathcal{H}_{MF} + \tfrac{1}{2}\textstyle\sum_{\mathbf{q}} \frac{n_f}{4m}\mathbf{q}^2\theta(\mathbf{q})\theta(-\mathbf{q}), \\ \mathcal{H}_I &= \textstyle\sum_{\mathbf{k},\mathbf{q},\sigma} m\mathbf{v}(\mathbf{k})\cdot\mathbf{v}_s(\mathbf{q})c^\dagger_{\mathbf{k}+\mathbf{q},\sigma}c_{\mathbf{k},\sigma}, \end{aligned} \tag{6.2}$$

where m is the free electron mass, $\mathbf{v}(\mathbf{k}) = \nabla_{\mathbf{k}}\xi_{\mathbf{k}}/\hbar$ is the normal-state group velocity, and $\mathbf{v}_s = \int d^2r e^{-i\mathbf{q}\cdot\mathbf{r}}\nabla\theta(\mathbf{r})/2m$ is the superfluid velocity.

Expressed in the basis of Ψ, $\mathcal{H}_I = \sum_{\mathbf{k},\mathbf{q}} \Psi^\dagger_{\mathbf{k},\mathbf{Q}} H_I(\mathbf{k},\mathbf{q}) \Psi_{\mathbf{k},\mathbf{Q}}$ where

$$\begin{aligned} H_I &\propto \begin{pmatrix} i\theta_{\mathbf{q}}\,\mathbf{q}\cdot\nabla_{\mathbf{k}}\xi_{\mathbf{k}} & 0 & 0 & 0 \\ 0 & i\theta_{\mathbf{q}}\,\mathbf{q}\cdot\nabla_{\mathbf{k}}\xi_{\mathbf{k}} & 0 & 0 \\ 0 & 0 & i\theta_{\mathbf{q}}\,\mathbf{q}\cdot\nabla_{\mathbf{k}}\xi_{\mathbf{k}+\mathbf{Q}} & 0 \\ 0 & 0 & 0 & i\theta_{\mathbf{q}}\,\mathbf{q}\cdot\nabla_{\mathbf{k}}\xi_{\mathbf{k}+\mathbf{Q}} \end{pmatrix} \\ &\approx i\theta_{\mathbf{q}}\,\mathbf{q}\cdot\nabla_{\mathbf{k}}\xi_{\mathbf{k}} \begin{pmatrix} 1 & 0 & 0 & 0 \\ 0 & 1 & 0 & 0 \\ 0 & 0 & -1 & 0 \\ 0 & 0 & 0 & -1 \end{pmatrix}. \end{aligned} \tag{6.3}$$

In deriving Eq. (6.3), we have taken the approximation $\xi_{\mathbf{k}+\mathbf{Q}} \approx -\xi_{\mathbf{k}}$ to simplify the calculation, which holds for electrons around the Fermi surface along the {100} and {010} axes where CDW couples most strongly with SC.

With Eq. (6.3), we can now write down the proper self-energy for the electrons:

$$\begin{aligned}\Sigma^*(\mathbf{k}) &= \textstyle\sum_{\mathbf{q}} H_I(\mathbf{k},\mathbf{q}) G(\mathbf{k}+\mathbf{q},\omega) H_I(\mathbf{k}+\mathbf{q},-\mathbf{q}) \\ &= \textstyle\sum_{\mathbf{q}} \frac{1}{16} \langle\theta_{\mathbf{q}}\theta_{-\mathbf{q}}\rangle\, (\mathbf{q}\cdot\nabla_{\mathbf{k}}\xi_{\mathbf{k}})(\mathbf{q}\cdot\nabla_{\mathbf{k}}\xi_{\mathbf{k}+\mathbf{q}}) \begin{pmatrix} G_{11}(\mathbf{k},\omega) & -G_{12}(\mathbf{k},\omega) \\ -G_{21}(\mathbf{k},\omega) & G_{22}(\mathbf{k},\omega) \end{pmatrix},\end{aligned} \tag{6.4}$$

where $G_{ij}(\mathbf{k},\omega)$'s are the (2×2) matrices composing the full Green's function

$$G(\mathbf{k},\omega) = \begin{pmatrix} G_{11}(\mathbf{k},\omega) & -G_{12}(\mathbf{k},\omega) \\ -G_{21}(\mathbf{k},\omega) & G_{22}(\mathbf{k},\omega), \end{pmatrix}.$$

In Eqs. (6.3) and (6.4), only the longitudinal phase fluctuations are retained because at $T = 0$ in the zero field limit, the transverse phase fluctuations are energetically very costly and therefore may be neglected. After summing over an infinite series of ring diagrams [Fig. 6.1(a)], the phase field correlation function $\langle\theta_{\mathbf{q}}\theta_{-\mathbf{q}}\rangle$ is given by [264]

$$\langle\theta_{\mathbf{q}}\theta_{-\mathbf{q}}\rangle \approx \frac{4m\,\omega_p}{\hbar\, n_s^{2D}\,\Omega}\,\frac{1}{q^2}, \tag{6.5}$$

where n_s^{2D} the two-dimensional superfluid density, ω_p the plasma frequency, and Ω the sample volume.

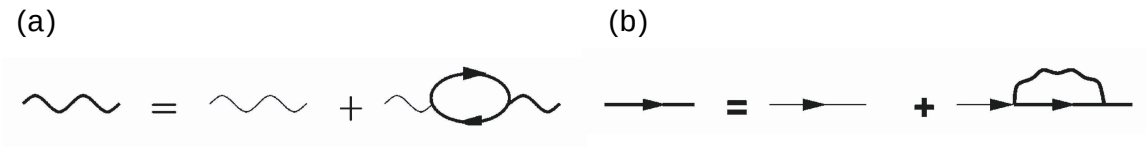

Figure 6.1: (From Figs. 3 and 4 of Ref. [262].) (a) The infinite sum of the ring diagrams for the superfluid velocity field propagator. (b) The Dyson's equation for the fermion Green's function. The thin (thick) wiggly line is the bare (full) velocity field propagator, and the thin (thick) solid line is the bare (full) fermion Green's function.

Thus, we obtain the full Green's function $G(\mathbf{k},\omega)$ self-consistently through the Dyson's equation

[Fig. 6.1(b)]:

$$
\begin{aligned}
G^{-1}(\mathbf{k},\tilde{\omega}) &= G_0^{-1}(\mathbf{k},\omega) - \Sigma^* \\
&= G_0^{-1}(\mathbf{k},\omega) - \eta \textstyle\sum_{\mathbf{q}} \frac{1}{q^2} \left(\mathbf{q}\cdot\nabla_{\mathbf{k}}\xi_{\mathbf{k}}\right)\left(\mathbf{q}\cdot\nabla_{\mathbf{k}}\xi_{\mathbf{k}+\mathbf{q}}\right) \begin{pmatrix} G_{11}(\mathbf{k},\tilde{\omega}) & -G_{12}(\mathbf{k},\tilde{\omega}) \\ -G_{21}(\mathbf{k},\tilde{\omega}) & G_{22}(\mathbf{k},\tilde{\omega}) \end{pmatrix} \\
&= \begin{pmatrix} \tilde{\omega}-\tilde{\xi}_{\mathbf{k}} & \tilde{\Delta} & \tilde{V} & 0 \\ \tilde{\Delta} & \tilde{\omega}+\tilde{\xi}_{\mathbf{k}} & 0 & -\tilde{V} \\ \tilde{V} & 0 & \tilde{\omega}-\tilde{\xi}_{\mathbf{k}+\mathbf{Q}} & \tilde{\Delta} \\ 0 & -\tilde{V} & \tilde{\Delta} & \tilde{\omega}+\tilde{\xi}_{\mathbf{k}+\mathbf{Q}} \end{pmatrix},
\end{aligned}
\tag{6.6}
$$

Here $\tilde{\omega}$ denotes the energy renormalized by the phase fluctuations, and $\eta \equiv m\omega_p/4\hbar n_s^{2D}\Omega q^2$ is a parameter indicative of the magnitude of fluctuations. Equation (6.6) can be solved self-consistently for each ω and each $\mathbf{k}$-value in the Brillouin zone. Summing over a finite phase space in $\mathbf{q}$ near each $\mathbf{k}$, we use the iterative Newton's method to find the corresponding $\tilde{\xi}_{\mathbf{k}}$, $\tilde{\omega}$, $\tilde{V}$ and $\tilde{\Delta}$ to the full Green's function $G(\mathbf{k},\tilde{\omega})$ [270]. The converged Green's function thus yields the spectral density function $A(\mathbf{k},\tilde{\omega}) \equiv -\mathrm{Im}\left[G(\mathbf{k},\tilde{\omega})\right]/\pi$ and the DOS $\mathcal{N}(\tilde{\omega}) \equiv \sum_{\mathbf{k}} A(\mathbf{k},\tilde{\omega})$.

In the case of $d_{x^2-y^2}$-wave SC, similar derivations can be made if we replace in Eq. (6.1) Δ by $\Delta_d(\cos k_x a - \cos k_y a)$ and V by the disorder-pinned $g^2 V_{SDW}$, where a is the square lattice constant, and g is the coupling strength between SDW and disorder. The periodicity $\mathbf{Q}$ of the charge modulations caused by the disorder-pinned SDW is twice that of the SDW.

6.2.2 Numerical results

For a given cuprate band structure with a known doping level, the quasiparticle DOS calculated from the aforementioned approach depends primarily on two variables: the ratio Δ/V and the magnitude of the quantum phase fluctuations represented by η. For an s-wave electron-doped superconductivity with $\Delta > V$, finite quantum phase fluctuations can induce substantial subgap DOS even if the mean-field SC and CDW orders are fully gapped, as illustrated in Fig. 6.2(a). Comparing the single-particle excitation spectrum derived from §6.2.1 with the BCS curve, we see

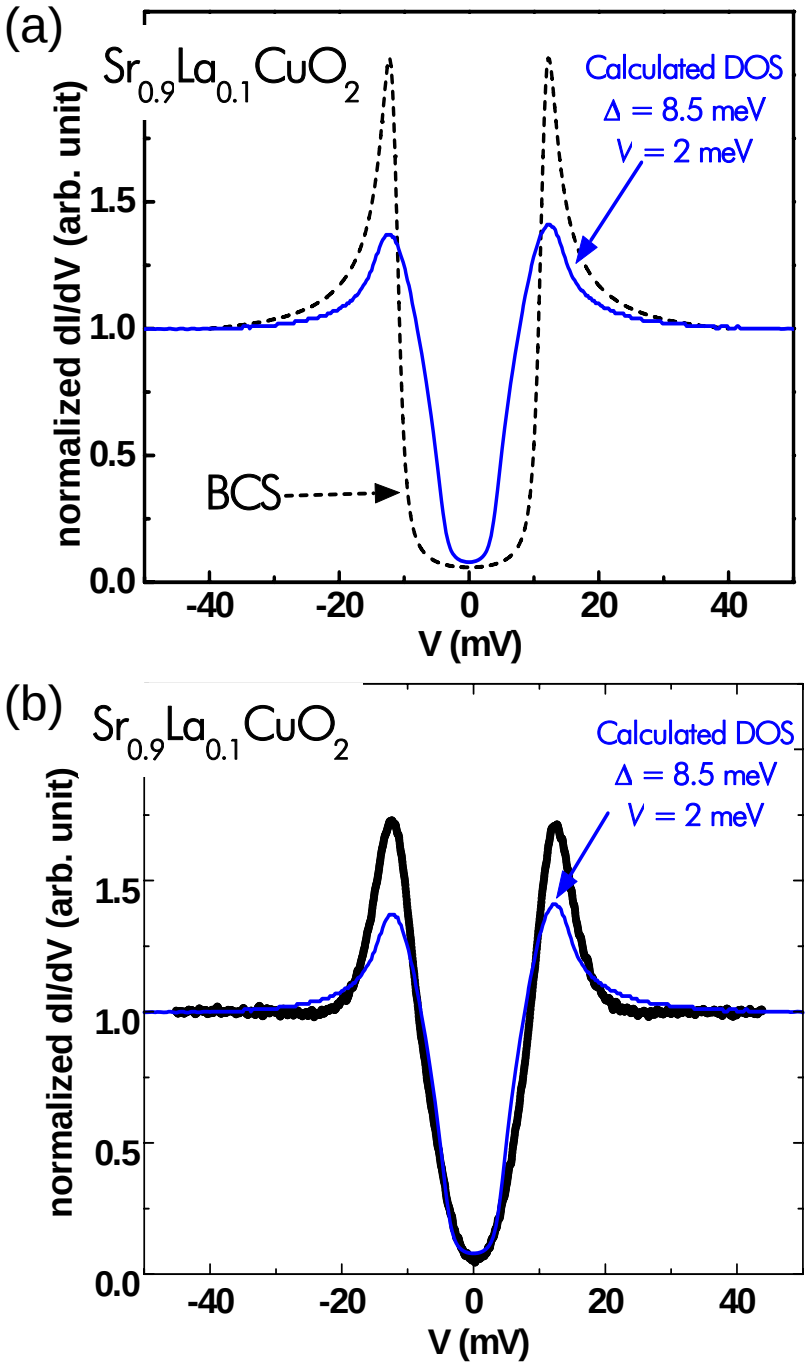

Figure 6.2: Comparison of the calculated quasiparticle DOS with experimental spectra on SLCO: (a) The calculated DOS for coexisting s-wave SC and CDW with quantum fluctuations is compared with the BCS prediction (dashed line). We note that finite subgap DOS can be induced by quantum fluctuations even if the mean-field DOS is fully gapped. (b) Momentum-independent quasiparticle tunneling spectrum of the electron-doped cuprate SLCO (thick line) is compared with the calculated DOS. The bare parameters are $\Delta = 8.5$ meV, $V = 2$ meV, and the fluctuation strength $\eta = 0.0001/16\pi$.

that, under finite quantum fluctuations, the spectral weight shifts from above the mean-field gap to lower energies and the spectral peaks are suppressed. The bare superconducting gap value and bare charge density wave energy for this set of simulation are chosen to be 8.5 meV and 2 meV, respectively, to match the experimentally observed peak position. The spectral peak of the phase-fluctuated SC with coexisting CDW locates at ~ 13.5 meV, but the effective gap $\Delta_{eff} = \sqrt{\Delta^2 + V^2}$ is only $\sim (9 - 11.5)$ meV when all uncertainties in fitting parameters are included. Therefore, in the presence of fluctuations, the subgap density of states is filled in and the peak-to-peak separation of the single-particle spectrum appears larger than the actual spectral gap, which is characteristic of any fluctuation-smeared tunneling spectrum.

In Fig. 6.2(b), we plot the normalized quasiparticle tunneling spectrum of SLCO with the simulation result. The calculated spectrum fits the low-energy excitations of the experimental data fairly well, while the calculated peak height is lower than the observed peak height. Since the calculated spectrum conserves the density of states when compared with the mean-field BCS prediction and yields a reasonable $2\Delta/k_BT_c \sim 4.85$ ratio, we believe that the simulation captures all major low-energy physics of SLCO and that the discrepancy in peak height between the calculated and the observed spectra may have originated from the tunneling matrix effect and the uncertainty in background normalization.

We further investigate how the quasiparticle tunneling spectra of an s-wave superconductor evolve under varying V/Δ ratio and a constant magnitude of quantum phase fluctuations. Given the degrees of phase fluctuation characterized by $\eta = 0.0001/16\pi$, the calculated spectra for $V/\Delta < 1$, such as those for $V/\Delta = 2.0/8.5$ and $V/\Delta = 8.0/8.5$, exhibit similar spectral characteristics [Fig. 6.3(a)]. They all exhibit substantial subgap low-energy excitations but no discernible satellite features. For a larger $V/\Delta > 1$, the satellite features designated by the red circle in Fig. 6.3(b) appear above the spectral gap, which is indicative of the coexisting CDW. Therefore, the absence of satellite features in the superconducting state tunneling spectra of electron-doped cuprates implies that the energy scale of the coexisting order is smaller than that of superconductivity. Consequently, as the temperature increases, the competing order vanishes before the system turns normal, which explains the absence

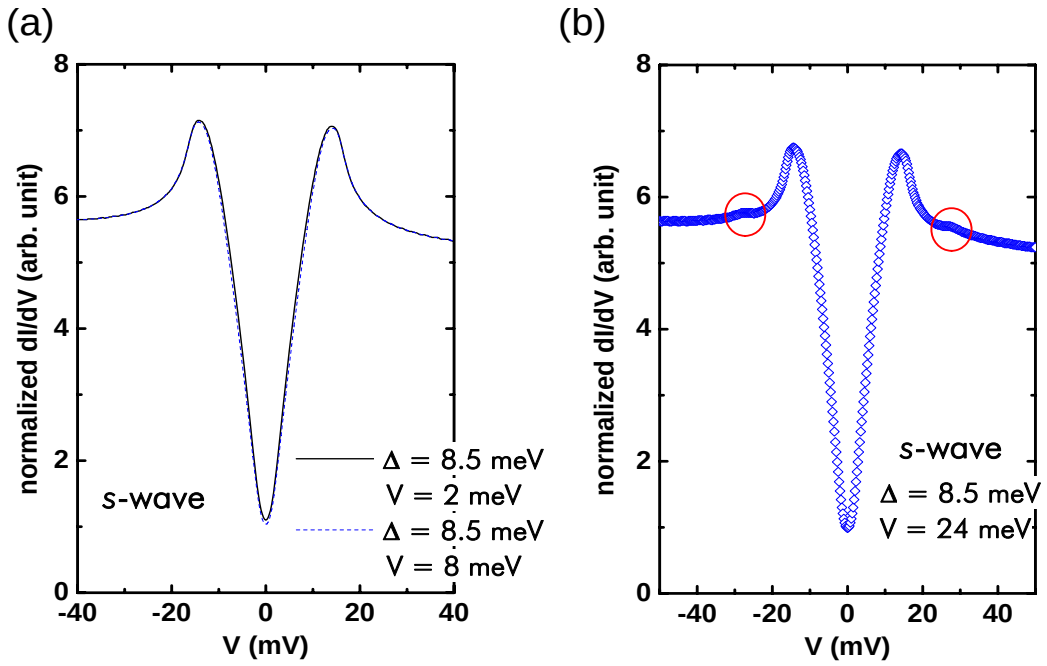

Figure 6.3: A scenario for the occurrence of the satellite features as the consequence of coexisting CO and SC in the ground state with $V \geq \Delta$: Evolution of the quasiparticle tunneling spectra for an s-wave superconductor from absence of the satellite features to appearance of which with increasing (V/Δ) and a constant magnitude of quantum phase fluctuations $\eta = 0.0001/16\pi$.

of pseudogap in their normal-state tunneling spectra.

For a $d_{x^2-y^2}$-wave hole-doped superconductors, we find that by taking into account a coexisting disorder-pinned density wave with $g^2 V_{SDW} > \Delta$, our model can reproduce the experimentally observed satellite features [as indicted by the red circles in Fig. 6.4(b)] in the limit of vanishing phase fluctuations [Fig. 6.4(a)]. The incorporation of varying degrees of quantum phase fluctuations would give rise to various types of "pseudogap"-like spectra revealed in the scanning tunneling spectra on Bi-2212 [Fig. 6.4(d)] [68]. A specific example that displays double peaks of comparable height is given in Fig. 6.4(c) to compare with the empirically observed double-peak structure, as indicated by the arrows in Fig. 6.4(d). Decreasing the phase fluctuations and CO would recover the sharp superconducting coherence peaks, as shown in spectra denoted by thin red lines in Fig. 6.4(d) and in Fig. 6.4(a). In contrast, increasing phase fluctuations while maintaining the strengths of both orders smears the double-peak feature into a big broad "pseudogap" peak as shown in Fig. 6.4(e). By comparing the calculated spectra of a d-wave hole-doped cuprate superconductor [Fig. 6.4(a,c,e)]

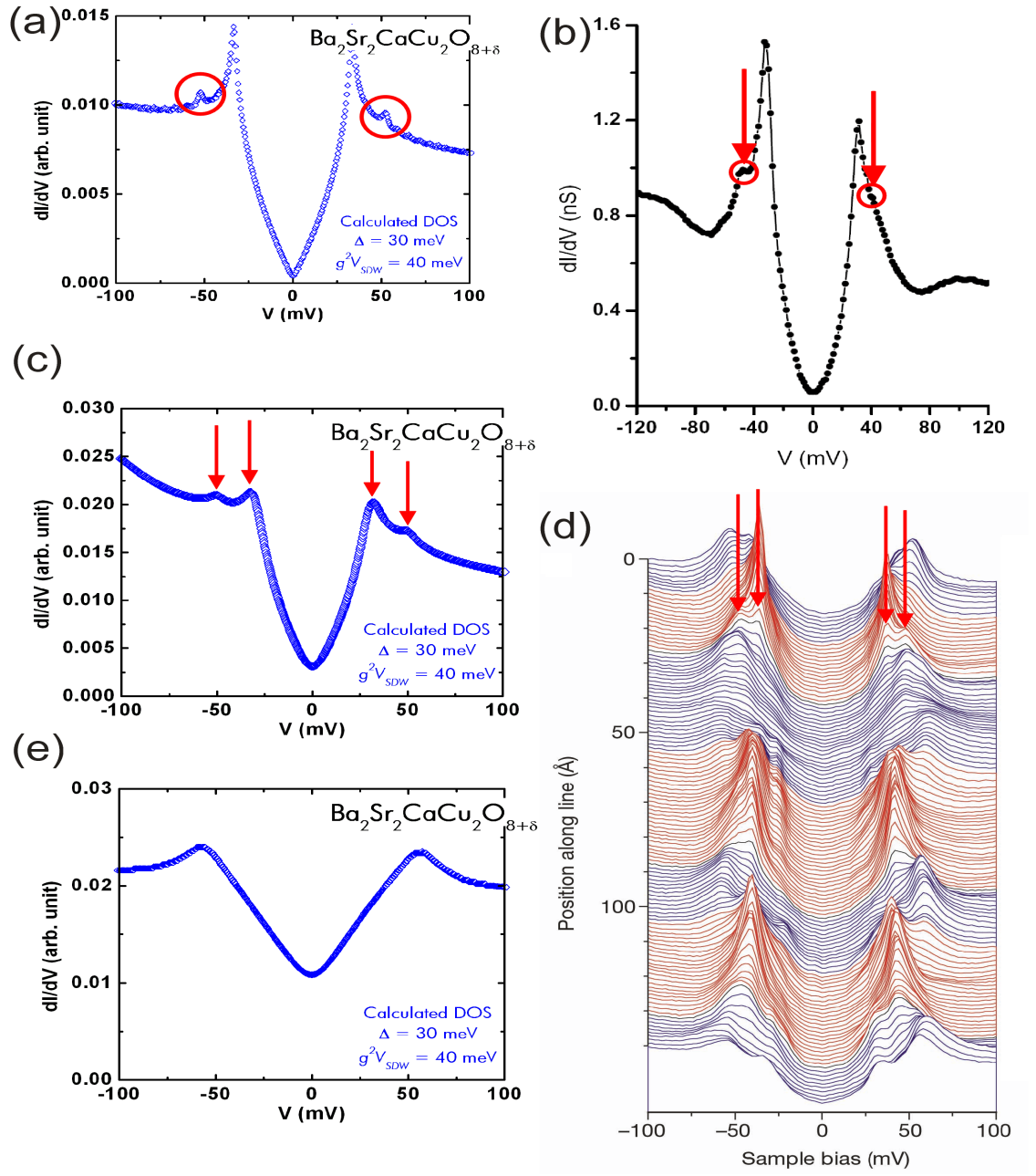

Figure 6.4: Comparison of the calculated quasiparticle DOS with experimental spectra on Bi-2212: (a) Calculated d-wave mean-field DOS using parameters $\Delta = 30$ meV, $g^2V_{SDW} = 40$ meV, and $\eta = 0$. (b) (Adapted from Fig. 2 of Ref. [183].) Quasiparticle c-axis tunneling spectrum of the hole-doped d-wave superconductor Bi-2212 in Ref. [183], showing satellite features as marked by arrows. (c) Calculated d-wave DOS with phase fluctuations using parameters $\Delta = 30$ meV, $g^2V_{SDW} = 40$ meV, and $\eta = 0.001/16\pi$. (d) (Adapted by permission from Macmillan Publishers Ltd: Nature [68], copyright (2002).) Quasiparticle c-axis tunneling spectrum of $Bi_2Sr_2CaCu_2O_x$ in Ref. [68], showing "pseudogap"-like features and the coexistence of two gaps as indicated by the red arrows. (e) Calculated d-wave DOS with phase fluctuations using parameters $\Delta = 30$ meV, $g^2V_{SDW} = 40$ meV, and $\eta = 0.0025/16\pi$. We note that the double-peak structure in (c) merges into one broad peak, yielding a pseudogap-like spectrum.

with the empirically observed "pseudogap"-like spectra [Fig. 6.4(d)] [68]], we see clearly that the nano-scale variations in the spectral gap of Bi-2212 originate from the interplay of the competing order with the phase-fluctuated superconducting order, whose fluctuation strength varies at nano-scale possibly due to random disorder in this high-2D system. The energy scale of the competing order is larger than that of superconductivity, and hence the spectral gap associated with the coexisting order sustains above the superconducting transition temperature, giving rise to the pseudogap observed in the normal-state tunneling spectra of Bi-2212 [54].

6.2.3 Summary

In summary, we recapitulate the implications of the coexistence of SC and CO on the origin of pseudogap phenomena and the satellite features in cuprate superconductors. For arbitrary values of Δ and V, the poles associated with $\mathcal{H}_{MF}$ in Eq. (6.1) generally give rise to two sets of peaks at $\omega = \pm\Delta_{\text{eff}}$ and $\omega = \pm\Delta$ in the quasiparticle DOS. For $\Delta \gg V$, we find that $\Delta_{\text{eff}} \approx \Delta$ so that only one set of peaks can be resolved in the quasiparticle spectra, particularly under finite quantum fluctuations. In this case, the magnitude of Δ_{eff} in the quasiparticle spectra is expected to decrease with increasing T and completely vanishes at T_c, which is consistent with the general findings in the electron-type cuprate superconductors [49, 16, 271]. On the other hand, for $V \geq \Delta$, two distinct sets of peaks can be resolved at $T \ll T_c$ and for limited quantum phase fluctuations. With increasing T or quantum phase fluctuations, the peaks at $\omega = \pm\Delta$ diminish while those at $\omega = \pm\Delta_{\text{eff}} \sim \pm V$ are broadened by fluctuations thus appear to remain nearly invariant in position, similar to the findings of pseudogap phenomena in underdoped $Bi_2Sr_2CaCu_2O_x$ (Bi-2212) cuprates above T_c [54]. In short, these results corroborate our conjecture that $V \ll \Delta$ is associated with the absence of pseudogap and the satellite features in electron-doped cuprates, whereas $V \geq \Delta_d$ is responsible for their presence in under- and optimally doped hole-doped cuprates. Thus, the experimental observation of non-universal pseudogap phenomena in the cuprates can be reconciled by coexisting CO and SC of different relative strengths.

6.3 Collective modes and quasiparticle interference on the local density of states of cuprate superconductors[1]

The presence of competing orders and the proximity to quantum criticality [249, 62, 202] have significant consequences on the unconventional low-energy excitation spectra of the cuprates, including weakened superconducting phase stiffness [73], the occurrence of excess subgap quasiparticle density of states (DOS) [49], and the presence (absence) of pseudogap [49, 54, 16] and Nernst effect in the hole (electron)-type cuprates above the SC transition [64, 65]. Other experimental observables of the coexisting orders involve various spin and charge ordering revealed in the neutron scattering and scanning tunneling spectroscopy measurements as mentioned in §1.2.3. In this section, we examine the effect of coexisting spin/charge density waves on recent scanning tunneling spectroscopic studies of the Fourier transformed (FT) quasiparticle local density of states (LDOS) in nearly optimally doped Bi-2212 [95, 97, 272] and find that while Bogoliubov quasiparticle interference [256, 258, 101, 273, 274, 275] apparently plays an important role in the observed FT-LDOS in the superconducting state, certain spectral details of the LDOS cannot be accounted for unless collective modes such as spin/charge density waves are considered [256, 258, 101]. More importantly, the observations of four high-intensity Bragg peaks remaining above T_c in the FT-LDOS map of Bi-2212 [99] cannot be reconciled with quasiparticles being the sole low-energy excitations. By comparing the experimental data to the calculated energy (E), momentum transfer (q) and temperature (T) dependence of the FT-LDOS modulations of a d-wave superconductor with random disorder, we conclude that collective modes such as spin/charge density waves are relevant low-energy excitations which contribute to the aforementioned LDOS modulations in Bi-2212.

6.3.1 Model

We begin our model construction by recalling that substantial nano-scale spectral variations are observed in the low-temperature tunneling spectroscopy of under- and optimally doped Bi-2212 single

[1] The main contents of this section are published as C.-T. Chen and N.-C. Yeh, *Phys. Rev. B* **68**, 220505(R) (2003).

crystals [Fig. 6.4(d)] [276, 67, 68, 194] which exhibits two types of spatially separated regions. In the last section, we have shown that for regions with double-peak or rounded hump-like "pseudogap" features at larger energies Δ_{eff}, quantum phase fluctuations resulting from pinned density waves coexisting with superconductivity are important, where as for region with sharp quasiparticle coherence peaks at smaller energies Δ_d, Bogoliubov quasiparticle spectra with a well-defined d-wave pairing order parameter $\Delta_{\mathbf{k}}$ dominate over the collective modes. Our model therefore assumes that, embedded in the predominantly superconducting regions, there are "puddles" of spatially confined "pseudogap regions" with a quasiparticle scattering potential modulated by the pinned density waves along the Cu-O bonding directions [§6.5]. The spatial modulations can be of either the 'checkerboard' pattern [256, 258] or 'charge nematic' with short-range stripes [277, 73] at a periodicity of four lattice constants, as inferred from neutron scattering experiments in a variety of p-type cuprates [84, 278, 279, 280, 281, 282, 85]. The calculation is implemented on a (400×400) sample area with either 24 randomly distributed point impurities or 24 randomly distributed puddles of charge modulations that cover approximately 6% of the sample area.[2]

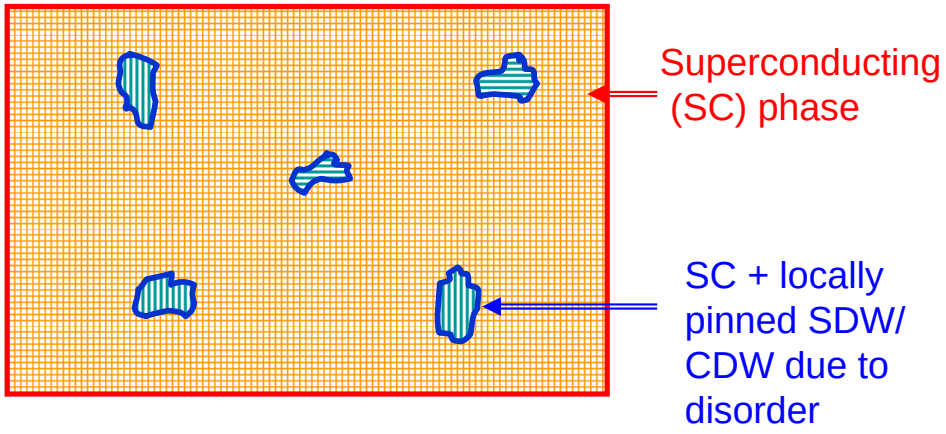

Figure 6.5: Disorder-pinned density waves forming "puddles" of "pseudogap" regions embedded in the predominantly superconducting region.

The Hamiltonian of the two-dimensional superconductor is given by $\mathcal{H} = \mathcal{H}_{BCS} + \mathcal{H}_{imp}$, where

[2]For simplicity, we do not take into account the effect of disorder on either suppressing the local pairing potential $\Delta_d(r)$ or altering the nearest-neighbor hopping coefficient (t) in the band structure of Bi-2212, although such effects reflect the internal structures of charge modulations [101, 273].

$\mathcal{H}_{BCS}$ denotes the unperturbed BCS Hamiltonian of the d-wave superconductor,

$$\mathcal{H}_{BCS} = \sum_{\mathbf{k}\sigma}(\epsilon_k - \mu)c^\dagger_{\mathbf{k}\sigma}c_{\mathbf{k}\sigma} + \sum_{\mathbf{k}} \Delta_{\mathbf{k}} \left[c^\dagger_{\mathbf{k}\uparrow}c^\dagger_{-\mathbf{k}\downarrow} + c_{-\mathbf{k}\downarrow}c_{\mathbf{k}\uparrow}\right],\ \Delta_{\mathbf{k}} \approx \Delta_d \cos 2\theta_{\mathbf{k}}, \tag{6.7}$$

and $\mathcal{H}_{imp}$ is the perturbation Hamiltonian associated with impurity-induced quasiparticle scattering potential [258, 273, 274]. In Eq. (6.7), Δ_d is the maximum gap value and $\theta_{\mathbf{k}}$ is the angle between the quasiparticle wavevector $\mathbf{k}$ and the anti-node direction. Using the T-matrix method, the Green's function $\mathcal{G}$ associated with $\mathcal{H}$ is given by $\mathcal{G} = \mathcal{G}_0 + \mathcal{G}_0 T \mathcal{G}_0$, where $\mathcal{G}_0$ is the Green's function of $\mathcal{H}_{BCS}$ and $T = \mathcal{H}_{imp}/(1 - \mathcal{G}_0\mathcal{H}_{imp})$ [*cf.* Appendix C]. We remark that the perturbative approach adopted here for the competing order is justifiable for low-energy (*i.e.*, $E < \Delta_d$) excitations in d-wave superconductors, because the gapless nodal Bogoliubov quasiparticles are the dominant low-energy excitations in this limit, as manifested in Fig. 6.4(a). In other words, the perturbative approach is a special case of the exact self-consistent treatment described in §6.2.

To proceed, we note that the Hartree perturbation potential for single scattering events in the diagonal part of $\mathcal{H}_{imp}$ is

$$V_\alpha(\mathbf{q}) = \sum_i V_{s,m} e^{i\mathbf{q}\cdot\mathbf{r}_i}$$

for non-interacting non-magnetic (V_s) and magnetic (V_m) impurities at locations $\mathbf{r}_i$ [274], whereas that for puddles with short stripe-like modulations centering at $\mathbf{r}_j$ is[3]

$$V_\beta(\mathbf{q}) = \sum_j V_0 e^{i\mathbf{q}\cdot\mathbf{r}_j} \frac{2\sin(q_{y,x}R_j)\sin(q_{x,y}R_j)}{q_{y,x}\sin(2q_{x,y})}, \tag{6.8}$$

and that for checkerboard modulations is

$$V_\gamma(\mathbf{q}) = \sum_j V_0 e^{i\mathbf{q}\cdot\mathbf{r}_j} \left[\frac{2\sin(q_yR_j)\sin(q_xR_j)}{q_y\sin(2q_x)} + (q_x \leftrightarrow q_y)\right]. \tag{6.9}$$

Here all lengths are expressed in units of the lattice constant a, R_j is the averaged radius of the

[3]For coexisting superconductivity and CDW, $V_\beta(\mathbf{q})$ represents the second-order effect of quasiparticle interference with pinned CDW. The first-order effect of CDW has been discussed in Ref. [101].

j-th puddle, and V_0 denotes the magnitude of the scattering potential by pinned collective modes. Empirically, for nearly optimally doped Bi-2212, R_j ranges from $5 \sim 10$ [68]. Here we take different values for R_j with a mean value $\langle R_j \rangle = 10$. In the context of our discussion in §6.2, the Hartree potentials contains information of the mean-field competing order and the self-energy correction that couples the superconducting phase fluctuations to the fermionic excitations of the coexisting state.

For simplicity, we neglect the energy dependence of $V_{\alpha,\beta,\gamma}$ and assume that V_s, V_m and V_0 are sufficiently small so that no resonance occurs in the FT-LDOS [273]. For sufficiently large scattering potentials, full T-matrix calculations become necessary as in Ref. [274]. However, large $V_{s,m}$ would result in strong spectral asymmetry between positive and negative bias voltages [274], which differs from experimental observation [95, 97, 272]. We also note that the energy dependence of $V_{\beta,\gamma}$ reflects the spectral characteristics of the collective modes and their interaction with quasiparticles and impurities. For instance, we expect $V_\gamma \sim \zeta g^2$ for pinned SDW, where ζ is the impurity pinning strength and g is the coupling amplitude of quasiparticles with SDW fluctuations [256, 258].

In the limit of weak perturbations, given the Hamiltonian and the scattering potentials $V_{\alpha,\beta,\gamma}(\mathbf{q})$, we find that the FT of the LDOS $\rho(\mathbf{r}, E)$ that involves elastic scattering of quasiparticles from momentum $\mathbf{k}$ to $\mathbf{k}+\mathbf{q}$ is

$$\begin{aligned}
&\rho_{\mathbf{q}}(\omega) = -\tfrac{1}{\pi N^2} \lim_{\delta\to 0} \textstyle\sum_{\mathbf{k}} V_{\alpha,\beta,\gamma}(\mathbf{q}) \times \\
&\Big\{ u_{\mathbf{k}+\mathbf{q}} u_{\mathbf{k}} \left(u_{\mathbf{k}+\mathbf{q}} u_{\mathbf{k}} \mp v_{\mathbf{k}+\mathbf{q}} v_{\mathbf{k}}\right) \mathrm{Im}\left[\tfrac{1}{(\omega - E_{\mathbf{k}} + i\delta)(\omega - E_{\mathbf{k}+\mathbf{q}} + i\delta)}\right] \\
&+ u_{\mathbf{k}+\mathbf{q}} v_{\mathbf{k}} \left(u_{\mathbf{k}+\mathbf{q}} v_{\mathbf{k}} \pm v_{\mathbf{k}+\mathbf{q}} u_{\mathbf{k}}\right) \mathrm{Im}\left[\tfrac{1}{(\omega + E_{\mathbf{k}} + i\delta)(\omega - E_{\mathbf{k}+\mathbf{q}} + i\delta)}\right] \\
&+ v_{\mathbf{k}+\mathbf{q}} u_{\mathbf{k}} \left(u_{\mathbf{k}+\mathbf{q}} v_{\mathbf{k}} \pm v_{\mathbf{k}+\mathbf{q}} u_{\mathbf{k}}\right) \mathrm{Im}\left[\tfrac{1}{(\omega - E_{\mathbf{k}} + i\delta)(\omega + E_{\mathbf{k}+\mathbf{q}} + i\delta)}\right] \\
&- v_{\mathbf{k}+\mathbf{q}} v_{\mathbf{k}} \left(u_{\mathbf{k}+\mathbf{q}} u_{\mathbf{k}} \mp v_{\mathbf{k}+\mathbf{q}} v_{\mathbf{k}}\right) \mathrm{Im}\left[\tfrac{1}{(\omega + E_{\mathbf{k}} + i\delta)(\omega + E_{\mathbf{k}+\mathbf{q}} + i\delta)}\right] \Big\}
\end{aligned} \tag{6.10}$$

in the first-order T-matrix approximation for infinite quasiparticle lifetime. Here N is the total number of unit cells in the sample, and Im[...] denotes the imaginary part of the quantity within the brackets, which is related to the equal-energy quasiparticle joint density of states. The upper (lower) sign in the coherence factor applies to spin-independent (spin-dependent) interactions. $u_{\mathbf{k}}$

and $v_{\mathbf{k}}$ are the Bogoliubov quasiparticle coefficients, $u_{\mathbf{k}}^2 + v_{\mathbf{k}}^2 = 1$, $u_{\mathbf{k}}^2 = [1 + (\xi_{\mathbf{k}}/E_{\mathbf{k}})]/2$, where $\xi_{\mathbf{k}} \equiv \epsilon_{\mathbf{k}} - \mu$, $E_{\mathbf{k}} = \sqrt{\xi_{\mathbf{k}}^2 + \Delta_{\mathbf{k}}^2}$, μ is the chemical potential, and $\epsilon_{\mathbf{k}}$ is the tight-binding energy of the normal state of Bi-2212 according to Norman *et al.* [283],

$$\begin{aligned}\epsilon_{\mathbf{k}} &= \tfrac{t_1}{2}(\cos k_x + \cos k_y) + t_2 \cos k_x \cos k_y + \tfrac{t_3}{2}(\cos 2k_x + \cos 2k_y) \\ &\quad + \tfrac{t_4}{2}(\cos 2k_x \cos k_y + \cos k_x \cos 2k_y) + t_5 \cos 2k_x \cos 2k_y,\end{aligned}$$

$t_{1-5} = -0.5951, 0.1636, -0.0519, -0.1117, 0.0510$ eV.

6.3.2 Numerical results

Using Eq. (6.10) and $V_{\alpha,\beta,\gamma}(\mathbf{q})$, we obtain the energy-dependent FT-LDOS maps in the first Brillouin zone for non-magnetic point impurities in Fig. 6.6 with two different superconducting gap values, $\Delta_d = 20$ and 40 meV, and $T = 0$. The most intensed modulation q-values are associated with the elastic scattering events connecting quasiparticle momenta k located around the tips of the constant-energy contours where the available phase space is maximized, as illustrated in Fig. 6.6(c). Comparing Fig. 6.6(a) with Fig. 6.6(b), we find that the polarity of the bias voltages does not change the primary features of the FT-LDOS plots, consistent with experimental findings. However, because of the directionality of the coherence factors $[u_{\mathbf{k+q}}u_{\mathbf{k}}\,(u_{\mathbf{k+q}}u_{\mathbf{k}} - v_{\mathbf{k+q}}v_{\mathbf{k}})]$, the intensities associated with $\mathbf{q}_B$ and $\mathbf{q}_C$ are much stronger than those of $\mathbf{q}_A$ [Fig. 6.6(a)(b)] and also in Fig. 6.7(a), which differs from the STM observation [95, 97] that reveals comparable intensities associated with $\mathbf{q}_A$ and $\mathbf{q}_B$, and weaker intensities with $\mathbf{q}_C$. Interestingly, the intensity of $\mathbf{q}_A$ becomes larger than that of $\mathbf{q}_B$ if one assumes magnetic point impurity scattering, as illustrated in Fig. 6.7(b). However, there is no evidence of magnetic scattering in the samples used in Refs. [95, 97]. In contrast, the presence of pinned collective modes, regardless of CDW or SDW, gives rise to much stronger intensities for $\mathbf{q}_A$ (by about two orders of magnitude), as shown in Fig. 6.8 for pinned SDW (with spin-dependent coherence factors). Thus, the empirical FT-LDOS maps [95, 97] cannot be solely attributed to quasiparticle scattering by non-magnetic point impurities and should contain contributions from the pinned density waves. For reference, an example of the real-space LDOS modulations corre-

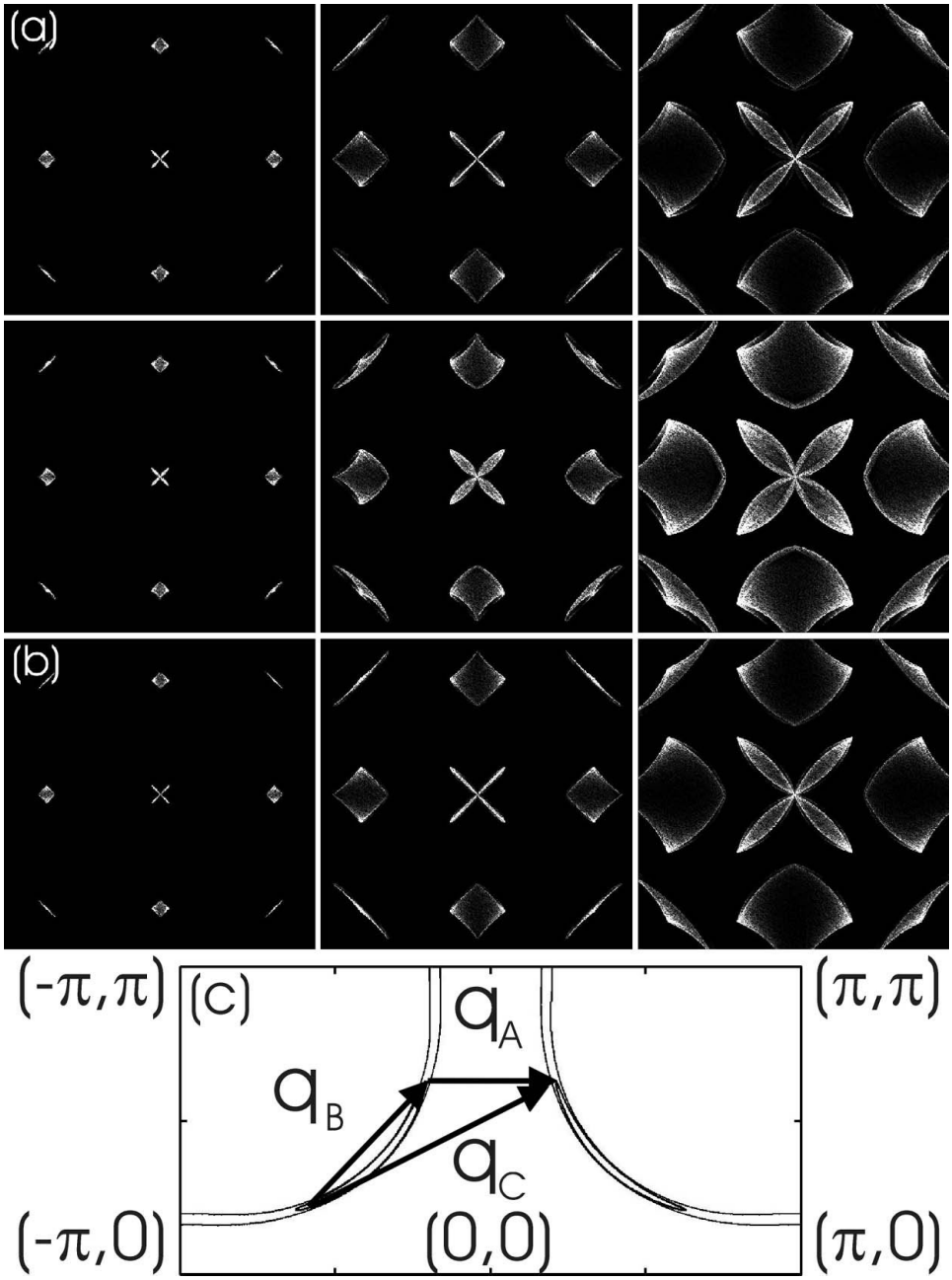

Figure 6.6: Calculated energy-dependent Fourier transform (FT) maps of quasiparticle LDOS in the first Brillouin zone with randomly distributed non-magnetic point defects using Eq. (6.10) and V_α: (a) $\Delta_d = 40$ meV and $(\omega/\Delta_d) = \pm 0.15, \pm 0.45, \pm 0.75$ (up and down from left to right); (b) $\Delta_d = 20$ meV and $(\omega/\Delta_d) = 0.15, 0.45, 0.75$ (left to right). (c) Schematic illustration of the equal-energy contours and representative modulation wavevectors $\mathbf{q}_A$, $\mathbf{q}_B$, and $\mathbf{q}_C$, which correspond to $\mathbf{q}_1$, $\mathbf{q}_7$, and $\mathbf{q}_2$ in Refs. [95, 97].

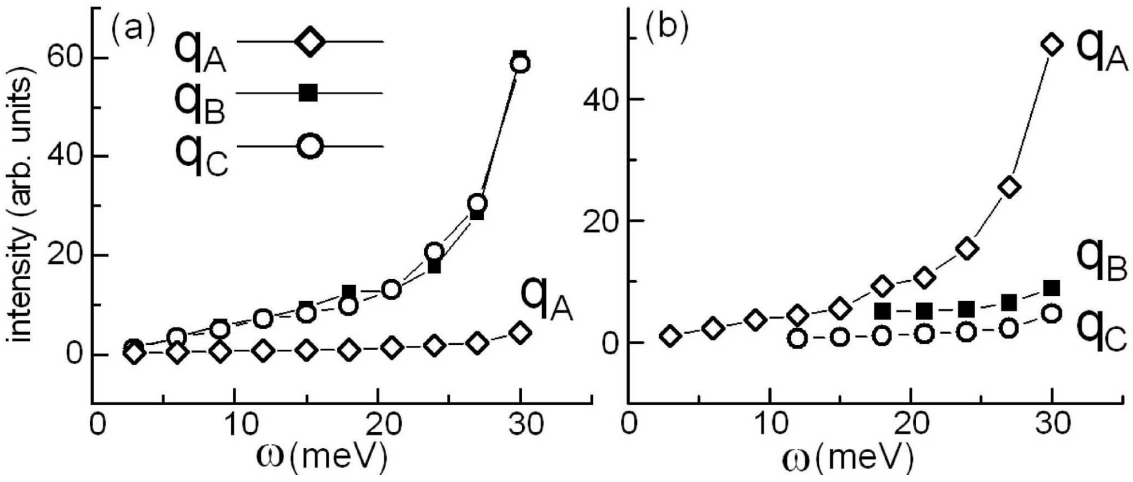

Figure 6.7: Evolution of the relative intensities of FT-LDOS with energy (ω) for q_A, q_B and q_C as defined in Fig.1(c) and V_s, V_m and V_0 all taken to be unity: quasiparticle scattering by (a) single non-magnetic point impurity, and (b) single magnetic point impurity.

sponding to quasiparticle scattering by the three types of random disorders $V_{\alpha,\beta,\gamma}(\mathbf{q})$ is included in Figs. 6.9(a)–(c), though a detail comparison between experiments and calculations must be done through the FT-LDOS maps.

The relevance of collective modes becomes indisputable when we consider the temperature dependence of the FT-LDOS. In calculating the FT-LDOS at finite temperatures, we assume $\Delta_d(T) = \Delta_d(0)\left[1-(T/T_c)\right]^{1/2}$, and the coherence factors change with temperature accordingly:

$$u^2_{\mathbf{k}} = \frac{1}{2}\left[1+\frac{\xi_{\mathbf{k}}}{E_{\mathbf{k}}}\right] = \frac{1}{2}\left[1+\frac{\xi_{\mathbf{k}}}{\sqrt{\xi^2_{\mathbf{k}}+\Delta^2_d(T)}}\right],\ v^2_{\mathbf{k}} = \frac{1}{2}\left[1-\frac{\xi_{\mathbf{k}}}{E_{\mathbf{k}}}\right] = \frac{1}{2}\left[1-\frac{\xi_{\mathbf{k}}}{\sqrt{\xi^2_{\mathbf{k}}+\Delta^2_d(T)}}\right].$$

The thermal smearing of quasiparticle tunneling conductance (dI/dV) is obtained by using

$$(dI/dV) \propto \left| \int \rho_{\mathbf{q}}(E)(df/dE)|_{(E-eV)} dE \right|,$$

where $f(E)$ denotes the Fermi function. As shown in Fig. 6.10(a), for point impurity scattering, the q-values contribute to the FT-LDOS map become significantly extended and smeared at $T = 0.75T_c$. In the limit of $T \to T_c^-$, the FT-LDOS contains hardly any feature except for the weak residual modulations encoding normal-state Fermi surface information. In contrast, pinned SDW yields

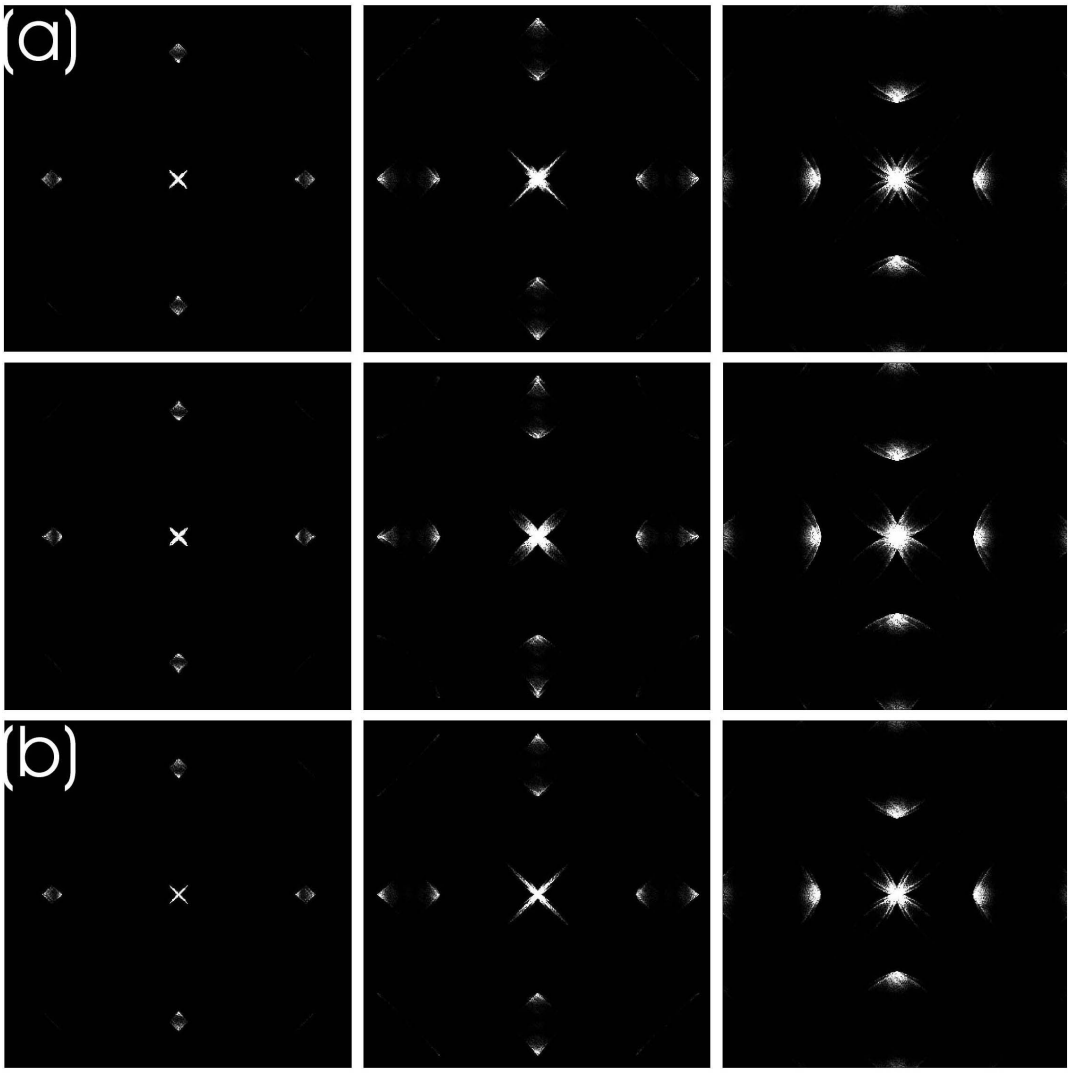

Figure 6.8: Energy-dependent FT-LDOS maps with randomly distributed pinned SDW using Eq. (6.10) and V_γ: (a) $\Delta_d = 40$ meV and $(\omega/\Delta_d) = \pm 0.15, \pm 0.45, \pm 75$, up and down from left to right; (b) $\Delta_d = 20$ meV and $(\omega/\Delta_d) = 0.15, 0.45, 0.75$, from left to right. The FT-LDOS does not exhibit discernible differences in the spectral characteristics except the total intensities if we simply replace V_γ by V_β and assume non-magnetic coherence factors in Eq. (6.10).

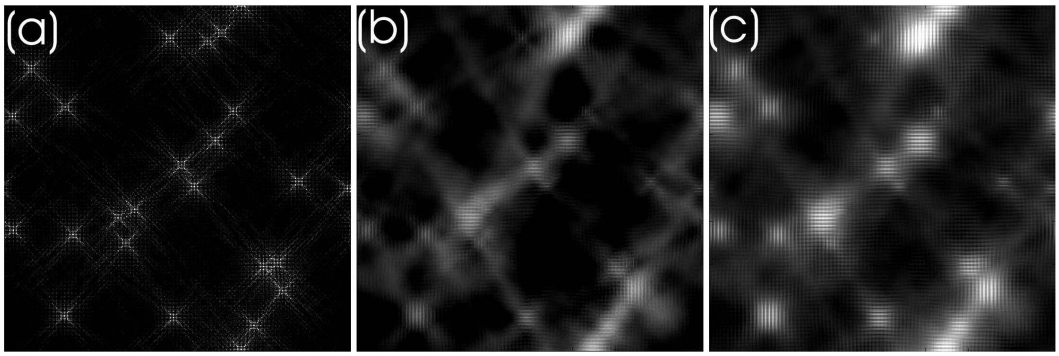

Figure 6.9: Real space quasiparticle LDOS for a (400×400) area at $T = 0$ due to scattering by (a) non-magnetic point impurities, (b) pinned CDW, and (c) pinned SDW, for $\Delta_d = 40$ meV and $\omega = 30$ meV.

strong intensities in the FT-LDOS map only at $\mathbf{q}_A$ for $T \geq T_c$, as shown in Fig. 6.10(b). The overall energy dispersion due to pinned SDW is weaker than that due to point impurities, as shown in Fig. 6.10(c) for $|\mathbf{q}_A|$ versus V(biased voltage) at both $T = 0$ and $T = T_c$. In particular, we note that the dispersion is further reduced at T_c. These findings are consistent with recent experimental observation of 4 nearly non-dispersive Bragg peaks above T_c by Vershinin *et al.* [99].

6.3.3 Summary

The energy, momentum, and temperature dependence of our calculated FT-LDOS in Figs. 6.6–6.10 is supportive of spatially modulated collective modes being relevant low-energy excitations in cuprates besides quasiparticles. In the superconducting state, the high intensities of the Bragg peaks along the principle axes cannot be explained by point-impurity as the sole scattering source. Furthermore, we must invoke the presence of pinned collective modes in order to account for the observation of 4 non-dispersive Bragg peaks in the FT-LDOS map above T_c.

6.4 Conclusion

In summary, we have analyzed the effect of quantum phase fluctuations and competing orders on cuprate superconductivity. By incorporating both superconductivity (SC) and competing orders (CO) in the bare Green's function and quantum phase fluctuations in the self-energy, we obtain

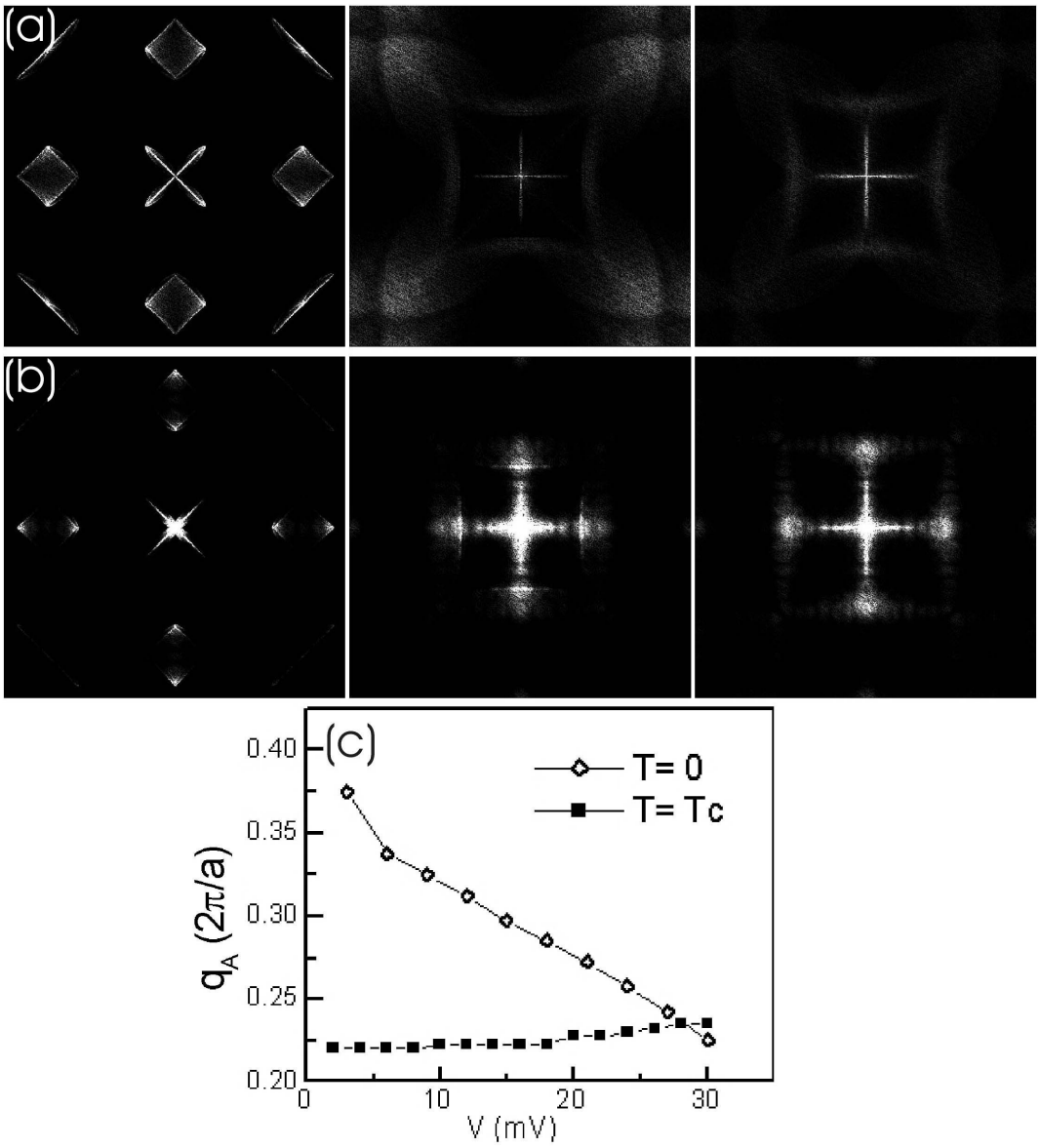

Figure 6.10: The FT-LDOS maps at $T = 0$, $0.75T_c$ and T_c (from left to right) for (a) point impurities $V_\alpha(q)$ and (b) pinned SDW $V_\gamma(q)$. We assume $\Delta_d(T) = \Delta_d(0)[1 - (T/T_c)]^{1/2}$, $\Delta_d(0) = 40$ meV, tunneling biased voltage = 18 mV, and $T_c = 80$ K. Besides temperature-dependent coherence factors, the thermal smearing of quasiparticle tunneling conductance (dI/dV) is obtained by using $(dI/dV) \propto |\int \rho_{\mathbf{q}}(E)(df/dE)|_{(E-eV)}dE|$, where $f(E)$ denotes the Fermi function. (c) $|q_A|$-vs.-V (biased voltage) dispersion relation for pinned SDW at $T = 0$ and T_c.

excess subgap quasiparticle density of states even for fully gapped SC and CO. Moreover, we find that the occurrence (absence) of pseudogap phenomena above T_c or H_{c2} in the hole (electron)-type cuprate superconductors may be a natural consequence of a competing order energy scale being larger (smaller) than the superconducting energy gap. We further investigate the modulations in the quasiparticle FT-LDOS of cuprates as a function of energy, momentum and temperature using the first-order T-matrix approximation in which the pinned CO is treated as a small perturbation. The latter approach is a special case of the self-consistent calculations and is justifiable when we consider the low-energy ($E < \Delta_d$) quasiparticle scattering in d-wave superconductors. Our results suggest that a full account for all aspects of experimental observation in hole-doped d-wave cuprates below T_c must include CO as relevant low-energy excitations besides Bogoliubov quasiparticles, and that only the pinned CO can account for the observed FT-LDOS above T_c.